Journal of Solid State Chemistry 184 (2011) 2751–2755

Contents lists available at SciVerse ScienceDirect

Journal of Solid State Chemistry

journal homepage: www.elsevier.com/locate/jssc

Phase equilibrium and intermediate phases in the Eu–Sb system

M.N. Abdusalyamova [a], I.G. Vasilyeva [b,*]

[a] Institute of Chemistry of Tajik Academy of Sciences, Ajni Str. 299/2, 734063 Dushanbe, Tajikistan
[b] Nikolaev Institute of Inorganic Chemistry, Russian Academy of Sciences, Siberian Branch, Lavrentiev Avenue, 3, 630090 Novosibirsk, Russian Federation

ARTICLE INFO

Article history:
Received 15 June 2011
Received in revised form
11 August 2011
Accepted 14 August 2011
Available online 23 August 2011

Keywords:
Eu-antimonides
Thermal analysis
Phase diagram

ABSTRACT

Rapid heating rate thermal analysis, X-ray diffraction, fluorescence spectrometry, and differential dissolution method were used to study the high-temperature phase equilibrium in the Eu–Sb system within the composition range between 37 and 96 at% Sb. The techniques were effective in determination of the vapor–solid–liquid equilibrium since intermediate phases except Eu_4Sb_3 evaporated incongruently after melting. A thermal procedure was developed to determine the liquidus and solidus lines of the $T-x$ diagram. Six stable phases were identified: two phases, $EuSb_2$ and Eu_4Sb_3, melt congruently at 1045 ± 10 °C and 1600 ± 15 °C, the Eu_2Sb_3, $Eu_{11}Sb_{10}$, Eu_5Sb_4, and Eu_5Sb_3 phases melt incongruently at 850 ± 8 °C, 950 ± 10 °C, 1350 ± 15 °C, and 1445 ± 15 °C, respectively. The exact composition shifting of Sb-rich decomposable phases towards Eu_4Sb_3, the most refractory compound, was determined. The topology of the Eu–Sb phase diagram was considered together with that of the Yb–Sb system.

1. Introduction

In recent years, considerable interest has been shown in $Yb_{14}MnSb_{11}$ and $Eu_{14}MnSb_{11}$ compounds, concerning not only their structure and composition, but also the physical properties making them suitable for use as high-temperature thermoelectric materials [1–4]. Such applications require the homogeneous $Yb_{14}MnSb_{11}$ and $Eu_{14}MnSb_{11}$ compounds and a comprehensive knowledge on their thermal stability over a wide temperature range. However, no efforts have been made to study the melting and evaporation of these compounds; the preparation of the pure and stoichiometric $A_{14}MnSb_{11}$ phases by heating the stoichiometric amounts of elements in welded Ta tubes or by crystallization from Sn metallic flux is still in doubt [1–4].

In a search for new convenient and efficient ways of preparing the $Yb_{14}MnSb_{11}$ and $Eu_{14}MnSb_{11}$ compounds, stability relations within the ternary *Ln*–Mn–Sb systems and mutual reactions between high refractory binary antimonides must be known. Of the Yb–Mn–Sb, Eu–Mn–Sb ternary and Yb–Sb, Eu–Sb binary systems, only the Yb–Sb system was investigated in close detail, apart from the upper $p-T$ stability of Yb antimonide phases [5,6]. Previous studies on the Eu–Sb system were focused only on the preparation and structural characterization of individual Sb-rich phases, like $EuSb_2$, Eu_2Sb_3, and $Eu_{11}Sb_{10}$ [7–11]. Nothing or little is known about the Eu-rich phases and the temperature stability range of all the Eu antimonides. Some experimental difficulties like extreme affinity for oxygen and high activity of Eu vapor towards the container materials prevent the production of homogeneous Eu compounds. No wonder that among binary systems including a rare earth metal and the group V–VI elements, the systems with Eu remain most commonly unstudied. It follows that a new type of experiment and specific tools are needed to study phase relations, especially in the metal-rich portion of the Eu–Sb system. Having experience in investigation of the $T-x$ diagrams of refractory compounds with volatile components, where the pressure is the active thermodynamic variable [12,13], we took a risk to examine the high-temperature portion of the Eu–Sb phase diagram (liquidus and solidus lines). This study was undertaken as a part of program on the preparation of high-quality ternary $Eu_{14}MnSb_{11}$ and binary Eu_4Sb_3 compounds that are of technical importance. The divalent state of Eu allows considering Eu_4Sb_3 as an analog of Zn_4Sb_3, which is among the most efficient thermoelectric materials [14].

2. Experimental

The binary Eu–Sb system was found to show similarities to the Yb–Sb system [5–8] therefore, our attention was centered on the composition range between 35 and 96 at% Sb, where main phases are located. 15 samples were prepared using a glove box with pure and dry argon. They had either a mixed composition or were represented by individual phases like Ln_5Sb_4, Ln_4Sb_3, and Ln_5Sb_3. The reactants Eu (99.9%, Aldrich) and Sb (99.9%, Aldrich) taken in

* Corresponding author. Fax: +7 383 330 94 89.
E-mail address: kamarz@niic.nsc.ru (I.G. Vasilyeva).

0022-4596/$ - see front matter © 2011 Elsevier Inc. All rights reserved.
doi:10.1016/j.jssc.2011.08.018

exactly weighed portions (total mass of 1.0 g) were ground well, pressed into pellets, sealed in evacuated quartz tube, and heated at 800 °C for 3–4 days with subsequent rapid quenching to 25 °C. This temperature was found to provide the reaction between the elements with minimum volatile losses and an equilibrium state for samples with high content of antimony ($\geq$50 at%) without resorting to further high-temperature reaction. For the Eu-rich samples ($\leq$50 at% Sb) to attain equilibrium, annealing in a closed inert container is needed at 1100 °C for 2–5 min, as is done with the refractory RE metal-rich antimonides and sulfides [5,15]. In our experiments, this procedure was performed in an open container, directly in the thermal apparatus just before recording the heating curve [12]. A small portion of the sample (2–4 mg) was placed on the bottom of the Mo crucible (6 mm long, hole ∅ 1 mm), where in the chamber at 1100 °C the internal vapor surrounding the sample was balanced without leakage by a high external gas pressure (~10 atm). Then the temperature was dropped to 800 °C, kept for 30 min, whereupon the sample was quenched rapidly.

The thermal apparatus for measuring of the solidus and liquidus temperatures is shown in Fig. 1. The Mo crucible (2) with the sample (1) was placed inside a tungsten heater of special geometry (4) in direct contact with a W/W-Re (20%) thermocouple (3). This assembly was put into a water-cooled chamber (5) filled with helium as a buffer gas. The recording system was a suitable IR photodiode mounted on a microscope (6) and measuring the emitted thermal radiation of the sample as a function of temperature through a quartz window (7). The phase transitions appeared as peaks on the thermal curves recorded in the $dU/d\tau - T$ coordinates, where $dU/d\tau$ is the time derivative of sample thermal radiation. The apparatus was calibrated against the melting points of substances recommended by ICTA: Sb (902 K), Ag (1234 K), Si (1693 K), and Pt (2045 K). The calibration was checked before each experimental run; e.m.f. values were measured for each substance (n=5–7) and expressed for each heating rate in a mathematical equation as a function of temperature, e.g., for a rate of 50 °C s^{-1}: $T=91.72+54.36x+0.00043x^4$. This calibration graph allows determining the temperature of the phase transitions with the accuracy of 1%.

The heating rate 3000 K/min and 7.0–10.0 atm of helium in the chamber were sufficient to prevent kinetically the vapor losses up to full melting of the sample, and the absence of the vapor condensate on the chamber window gave proof to the point. In this case, the measured liquidus points are consistent with the unchanged starting composition of the sample. To identify phase transitions, the sample was quenched from a desired temperature with subsequent determination of mass and composition of the vapor condensate and microscopic examination of the residue microstructure (partial or complete melting). This strategy was also used to study the thermal stability of Eu antimonides through their response to slow heating, when phase state of the initial sample changed due to progressing incongruent evaporation.

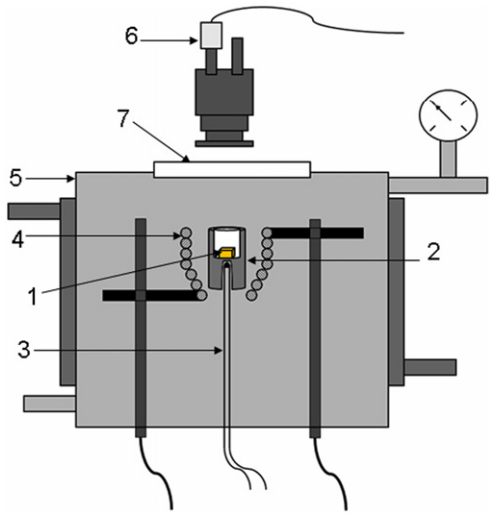

Fig. 1. Apparatus for investigation of melting and evaporation of Eu antimonides.

The elemental composition of Eu antimonides was determined by the X-ray fluorescence spectrometry using the Eu and Sb oxides as internal standards. The quantitative atomic ratio Eu:Sb in the vapor condensate was determined with inductively coupled plasma mass spectrometry (ICP-MS) using an ELEMENT mass spectrometer (Finnigan MAT) after dissolving in a solvent like 25 ml HNO_3+75 ml H_2O+2 g tartaric acid as a complexing agent for Sb.

The powder X-ray diffraction technique (XRD) with a DRON-3M diffractometer (Ni-filtered Cu$K\alpha$ radiation, 2θ=5–90°, step 0.02°, counting time of 15 s) was used to identify the Sb-rich samples based on the available powder structure data [7–11].

For lack of any structural data on the Eu-rich samples, the differential dissolution (DD) technique was used as the phase analysis of multiphase inorganic solids. This method identifies compounds from their elemental composition, which is the same primary attribute for substances as their structure. The DD strategy and technique are described in detail elsewhere [16]. The Eu–Sb sample is dissolved in a solvent flow (aqua regia:water=1:1) with the temperature continuously increasing from 25 to 60 °C to prove sequential dissolution of phases from heterogeneous mixture. The Eu and Sb amounts passing into solution are monitored by an ISP AE spectrometer every 5 s until a complete dissolution of the sample. The kinetic curves for the dissolution of Eu and Sb elements and their atomic ratio Sb:Eu are plotted as a time function. Simple stoichiographic calculations result in determination of empirical formulas of the phases and their amounts as areas under the phase dissolution curves. It was possible to find empirical formula and content of the phases with an error $\leq$5%.

3. Results

The elemental composition, phase identification, and thermal characteristics of the Sb-rich samples prepared from pure elements at 800 °C are given in Table 1. According to analytical data, the sum of Eu and Sb elements is almost 100% (error $\pm$0.4%) that is the samples are free from any oxide by-products. Their real compositions are fairly close to the nominal compositions considering the error of weighing and a small metal vapor loss caused by the interaction with a quartz container. The chemical analysis identifies the samples as heterogeneous, except the 66.6% one, which is confirmed by XRD. The powder X-ray diffraction patterns were in agreement with the reported structural data for $EuSb_2$ (PDF no. 71-1367), Eu_2Sb_3 (PDF no. 35-1024), and $Eu_{11}Sb_{10}$ (PDF no. 33-99). No other characteristic peaks of impurities like Eu and Sb oxides or antimony were observed.

Thermal effects on the heating curves recorded under equilibrium conditions (without vapor leakage) are shown in Fig. 2. It can be seen that for samples with Sb compositions 88, 92, and 96 at% the eutectic points appear at 605 °C, and liquidus temperatures (complete melting) occur at 800, 700, and 625 °C, respectively. $EuSb_2$ was found to melt congruently at 1045 °C, and the vapor condensate occurs only after melting. Samples with Sb compositions between 66.6% and 60% show coexistence of $EuSb_2$ and Eu_2Sb_3; the eutectic points appear at 815 °C, and Eu_2Sb_3 melts incongruently at 850 °C. In samples with Sb

Table 1
Characteristics of the Sb-rich samples.

Analytical data, mass%, **Real composition**, atom% Sb	XRD data	Temperature and type of thermal effect, °C, $n=7$–10, $\sigma=\pm1\%$
Anal.: Eu 38.4+Sb 61.8=100.2% **66.7** (66.6%=$EuSb_2$)	$EuSb_2$	1045—complete melting
Anal: Eu 39.9+Sb 60.4=100.3% **65.4** (=$EuSb_2+Eu_2Sb_3$)	Eu_2Sb_3 $EuSb_2$	820—partial melting 880 – complete melting
Anal. Eu 57.6+Sb 42.5=100.1% **62.8** (= $EuSb_2+Eu_2Sb_3$)	Eu_2Sb_3 $EuSb_2$	815—surface melting, 850—partial melting, 920—complete melting
Anal. Eu 54.1+Sb 45.8=99.9% **55.8** (=$Eu_2Sb_3+Eu_{11}Sb_{10}$)	Eu_2Sb_3 $Eu_{11}Sb_{10}$	845 and 950—partial melting, 1080—complete melting
Anal. Eu 57.9+Sb 42.0=99.9% **47.4** (47.6%=$Eu_{11}Sb_{10}$)	$Eu_{10}Sb_{11}$+un-indexed lines	950 and 1350—partial melting 1400—complete melting
59.6 (=$Eu_2Sb_3+Eu_{11}Sb_{10}$)	Eu_2Sb_3 $Eu_{11}Sb_{10}$	850—partial melting 950—complete melting
50 (=$Eu_2Sb_3+Eu_{11}Sb_{10}$)	Eu_2Sb_3 $Eu_{11}Sb_{10}$	850, 945—partial melting, 1340—complete melting
88.0 (=$EuSb_2$+Sb)	$EuSb_2$+Sb	605—surface melting, 805—complete melting
92.0 (=$EuSb_2$+Sb)	$EuSb_2$+Sb	600—surface melting, 700—complete melting
96.0 (=$EuSb_2$+Sb)	$EuSb_2$+Sb	625—complete melting

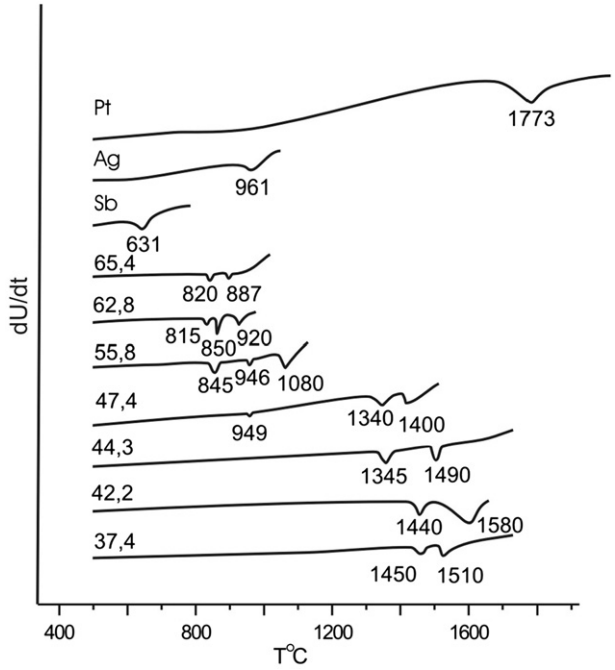

Fig. 2. Thermal heating curves of references and samples with Sb composition in at%.

compositions between 60 and 47.6 at%, Eu_2Sb_3 coexists with $Eu_{11}Sb_{10}$, and the peritectic reaction for $Eu_{11}Sb_{10}$ was observed at 950 °C. To construct correctly the liquidus line for the samples with 44–64 at% Sb, the vapor losses were quantitatively determined by the analytical procedure and the starting compositions were corrected for the difference. With the heating rate 3000 K/min and 10.0 atm of helium in the chamber, the losses varied from 0.2% to 0.6% of the total weight depending on the temperature interval between the corresponding peritectic and liquidus points.

Preparation of the Eu-rich samples included two steps: a prolonged heating at 800 °C and a short annealing at 1100 °C, after which the difference between the initial and the terminal compositions was determined chemically and the phases were identified due to the appropriate melting point peaks on the heating curves. Table 2 lists the results of both steps of the heating experiments. According to the analytical data, the Eu-rich samples synthesized at 800 °C were free from oxygen, with compositions differing only slightly from the nominal values. However, their X-ray powder diffraction patterns (not shown here) were quite complex and did not agree with any known ICPDS cards of possible Yb antimonides with the same stoichiometry, although many similarities in the patterns were apparent. Most likely, no phase-pure compounds but a mixture of phases formed at 800 °C even after prolonged heating of the samples.

In the absence of structural data, identification of the Eu-rich phases by the DD method was of prime importance. The dissolution curves of Eu and Sb elements and the atomic ratio Sb:Eu recorded as a time function are depicted in Fig. 3. A prolonged linearity of the Sb:Eu atomic ratio equal to 0.8, 0.75, and 0.6 identified the phases of the Eu_5Sb_4, Eu_4Sb_3, and Eu_5Sb_3 composition, respectively. The content of these phases was determined to be 95 ± 4 mass%. At the same time, a disruption of the linearity exceeding the error level is observed in the initial part of the Sb:Eu ratio in Fig. 3a and in the initial and end parts of the ratio in Fig. 3b, which indicates spatial homogeneity of the samples with impurity phases. The initial Sb:Eu ratio varies from 1.05 to 0.8 (Fig. 3a) and from 0.88 to 0.75 (Fig. 3b) indicating that Sb content in these impurity phases exceeds that in the main phases Eu_5Sb_4 and Eu_4Sb_3. Since in the end part (Fig. 3b) the Sb:Eu ratio decreases from 0.75 to 0.60, the impurity phase is enriched with Eu as compared to Eu_4Sb_3. Empirical formulas for the impurity phases were not found here because of variable character and short range of all these parts. However, the impurity phases were assigned to $Eu_{11}Sb_{10}$ and Eu_5Sb_3 due to melting points measured at 950 and 1445 °C on

Table 2
Characteristics of the Eu-rich samples before and after high-temperature annealing.

Analytical data, mass%, **Real composition,** ±0.4 at% Sb	DD data Content, mass%	Temperature and type of thermal effect, °C, n=7–10, $\sigma = \pm 1\%$
Before annealing:	Eu_5Sb_4—95%	950—surface melting
Anal. 39.1+60.8=99.9%	Impurity phases ~4%	1350—partial melting
44.6 (44.4=Eu_5Sb_4)		1500—complete melting
After annealing:		
Weight loss—0.12 mass%		1345—partial melting
Vapor ratio Eu:Sb=1:200		1490—complete melting
44.3%		
Before annealing:	Eu_4Sb_3—95%	945—surface melting,
Anal. 36.9+62.7=99.6%	Impurity phases ~4%	1445—partial melting
42.4 (42.8=Eu_4Sb_3)		1540—complete melting
After annealing:		
Weight loss—0.3		1440—partial melting
Vapor ratio Eu:Sb=1:200		1580—complete melting
42.2		
Anal. 32.8+67.4=100.2%	Eu_5Sb_3—98%	1445—partial melting
37.5 (37.5=Eu_5Sb_3)		1520—complete melting
After annealing:		
Weight loss—0.15%		
Vapor ratio Eu:Sb=1:100		1450—partial melting
37.4%		1510—complete melting

the heating curves for samples with Sb compositions 44.6% and 42.4% (Table 2, before annealing). Annealing of these samples at 1100 °C above incongruent melting point of $Eu_{11}Sb_{10}$ produces a liquid favorable for attaining an equilibrium. The composition of the equilibrated samples is gently shifted (44.3% and 42.2%) to transform into pure Eu_5Sb_4 and a mixture of Eu_4Sb_3 with a minor amount of Eu_5Sb_3 (Table 2, after annealing). Unfortunately, it was difficult to extract these melted samples from the Mo crucible (the wetting effect) for the structural study. So, the problem of structural identification of the Eu-rich phases remains to be solved.

Under equilibrium conditions (the heating rate 3000 K/min and 10.0 atm of helium), the Eu_5Sb_4 phase was found to melt incongruently at 1350 °C, forming an antimony-rich liquid and solid Eu_4Sb_3. For Eu_5Sb_3, the peritectic temperature of 1445 °C results in the equilibrium of solid Eu_4Sb_3 with a Eu-rich liquid. The liquidus temperatures for samples with 44.3 and 37.4% Sb and vapor losses about 0.6% lie at 1490 and 1510 °C, respectively. The composition 44.3% shows two peaks identified as the peritectic melting of Eu_5Sb_3 at 1440 °C and the liquidus point at 1586 °C.

Thermal behavior of the samples with the compositions 55.8%, 47.6%, 44.4%, and 37.5% Sb was studied in detail as a response to slow heating to the liquidus temperatures. The amount and composition of the vapor were determined quantitatively; the chilled products were examined with a microscope. This revealed a weight loss between 0.2% and 7.3%, and variation of the vapor atomic Eu:Sb ratio between 1:260 and 1:150 for Sb-rich liquids (44–55% Sb) and between ~1:50 and 1:35 for the Eu-rich ones (37–42% Sb). Antimony remains the predominant vapor species in all cases, although the boiling points for Eu and Sb are close to each other [17]; therefore, the initial Sb-rich compositions shift gradually in the Eu-rich portion of the Eu–Sb diagram. The composition 55.8% Sb is thermally decomposed in two steps via the formation of Eu_5Sb_4 below 1350 °C and Eu_4Sb_3 above this temperature. The solid particles, being in equilibrium with a Sb-rich liquid, are distributed over the surface melt and transformed to a homogeneous melt only at the liquidus temperature. Real

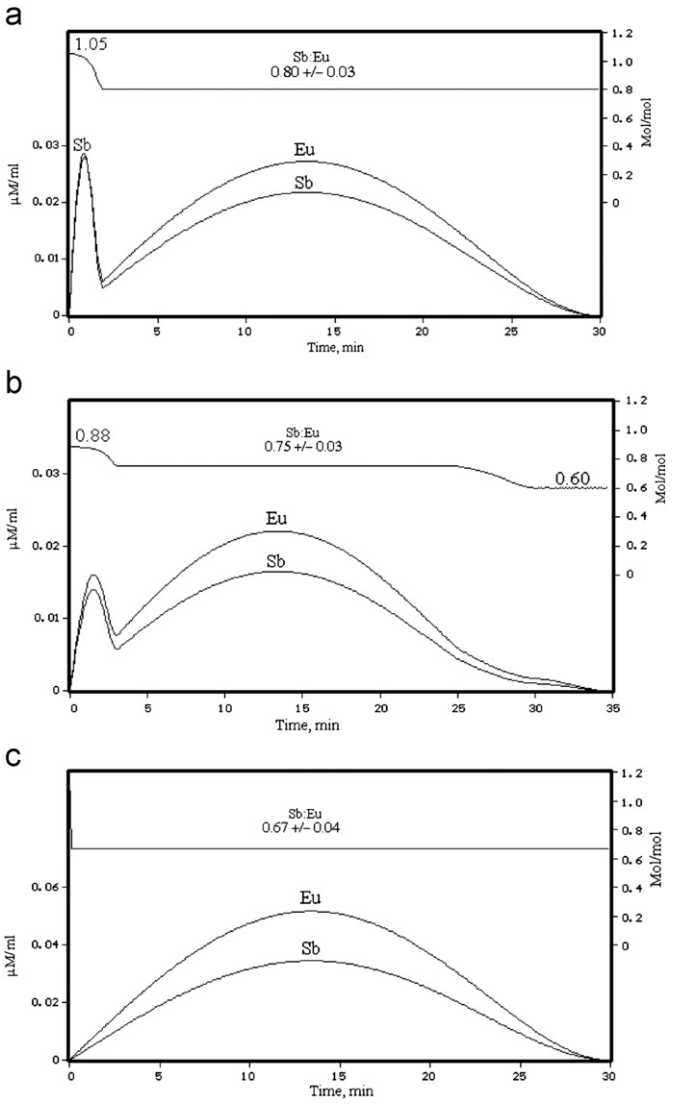

Fig. 3. Kinetic curves of the Sb and Eu dissolution (μmol/ml) and Sb:Eu atomic ratio as a time function for the samples with Sb compositions: 44.6 at% (a), 42.4 at% (b), and 37.4 at% (c).

compositions and the corresponding liquidus temperatures are listed as a function of heating time in Table 3. It is seen that the composition shift of all the samples, except 37.5%, is limited by the Eu_4Sb_3 composition. Melting of Eu_4Sb_3 was found to be congruent at 1600 °C with a singular point and a well-defined maximum on the liquidus line, which is characteristic of Eu_4Sb_3 as a stable chemical compound. The well reproducible melting temperature independent of the heating time is an evidence of congruent evaporation of Eu_4Sb_3 with a narrow composition range at higher temperatures.

The condensed phase diagram of the Eu–Sb system with the liquidus and solidus lines is shown in Fig. 4 within the composition range between 37 and 96 at% Sb. Our study, using a method to balance the vapor pressure in a quasi-closed system, allowed the existence of a high temperature region in both metal-rich and antimony-rich portions of the Eu–Sb system to be presented, while the solidus and liquidus lines of the Yb–Sb system were shown only schematically [5]. In our experiments, the identification of the phases was based on distinctions in their composition, volatility, and melting points, although the Sb-rich phases were characterized also structurally. The absence of structural data for the Eu-rich compounds gave us no way to study lower

Table 3
Compositional shift of the samples as a function of heating time.

Sample 55.8% Sb (=Eu_2Sb_3+$Eu_{11}Sb_{10}$)					
Composition	10 s→55.8;	15 s→55.0;	35 s→51.0;	60 s→48.6;	90 s→42.8;
Liquidus point, °C	1050	1190	1270	1335	1600
Sample 47.4 (=$Eu_{11}Sb_{10}$+Eu_5Sb_3)					
Composition	10 s→47.4;	15 s→47.0;	60 s→42.8;	90 s→42.8;	
Liquidus point, °C	1360	1420	1610	1608	
Sample 44.4(=Eu_5Sb_4+Eu_4Sb_3)					
Composition	10 s→44.4;	25 s→43.0;	60 s→42.8;		
Liquidus point,°C	1510	1586	1596		
Sample 37.5 (=Eu_5Sb_3)					
Composition	10 s→37.5	30 s→37.0.			
Liquidus point,°C	1520	1510			

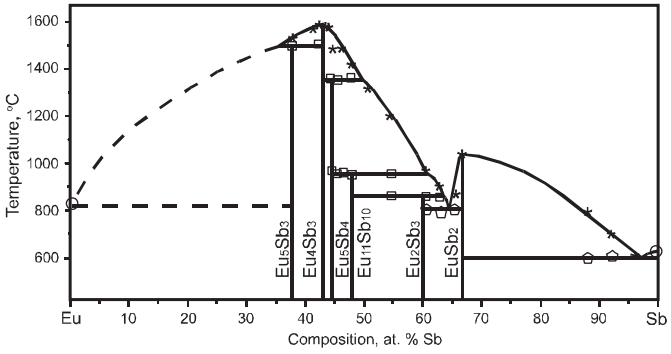

Fig. 4. The condensed phase diagram for the system Eu–Sb. Symbols: *—liquid; □—liquid and solid, △—eutectics, ○—melting points of the elements.

temperature phase equilibrium. Nevertheless, the stable phase formulas determined for the Eu–Sb system were identical with those observed in the subsolidus phase diagram of the Yb–Sb system [5,6], except Yb_2Sb_3, the existence of which is still doubtful. We also verified the occurrence of $Eu_{11}Sb_{10}$, an analog to $Yb_{11}Sb_{10}$, which is typical only of the Eu and Yb systems. Such compounds have not been synthesized in other rare earth metal–antimony systems. In addition, the high-temperature range of the diagram is or can be assumed to be new and very interesting for the production of materials of technical importance. So, the strongly stoichiometric Eu_4Sb_3 can be prepared via decomposition of Sb-rich compounds instead of direct synthesis from pure elements with ill effects; a direct reaction between Eu_4Sb_3 and Mn may be attractive to produce a homogeneous $Eu_{14}MnSb_{11}$ compound.

4. Conclusions

The study of the binary Eu–Sb system is complicated by a strong evaporation process occurring after melting of intermediate phases, which indicates the vapor–solid–liquid equilibrium in the high-temperature region of the Eu–Sb phase diagram. Progress in the study of the liquidus and solidus lines of this $T-x$ diagram was made due to unique ability of a new thermal technique, which is promising for investigation of the solid–liquid–vapor equilibrium. Precise measurement of the melting points of decomposable samples was performed in two ways: creating rigid conditions (heating rate of 3000 °C per minute and helium pressure of 10 atm) to preserve the initial composition up to complete melting, and checking quantitatively the composition and amount of the vapor when the initial composition is shifted due to incongruent evaporation of the sample. Thermal experiments as a response to rapid and slow heating of the samples with examination of their melting and evaporation behavior were implemented by plotting the liquidus–solidus lines of the $T-x$ diagram for samples within the composition range between 96 and 37 at% Sb.

Acknowledgments

This work was partly supported by the International Science & Technology Center (ISTC), Project T-1597. The authors thank Dr. R. Nikolaev (Institute of Inorganic Chemistry, Novosibirsk) for his kind help in preparation of the paper.

References

[1] I. Fisher, T. Wiener, S. Bud'ko, P. Canfield, Phys. Rev. B 59 (1991) 13829.
[2] Y. Chan, M. Olmstead, S. Kauzlarich, Chem. Mater. 10 (1998) 3583.
[3] A. Holm, T. Ozawa, S. Kauzlarich, S. Morton, G. Waddill, J. Tobin, J. Solid State Chem. 178 (2005) 262.
[4] R. Brown, S. Kauzlarich, F. Gascoin, G. Snyder, Chem. Mater. 18 (2006) 1873.
[5] R. Bodnar, H. Steinfink, Inorg. Chem. 6 (1967) 327.
[6] T.B. Massalski (Ed.), Binary Alloy Phase Diagrams, 2nd ed., 3 1990 3317.
[7] S. Solmelezer, D. Schwarzenbach, F. Hulliger, Z. Naturforsh. 34 (1979) 1213.
[8] B. Taylor, L. Calvert, Y. Wang, J. Appl. Crystallogr. 12 (1979) 249.
[9] B. Taylor, L. Calvert, J. Less Common Met. 57 (1978) 39.
[10] G. Chapuis, F. Hulliger, A. Schmeltzer, J. Solid State Chem. 31 (1980) 59.
[11] F. Hulliger, A. Schmeltzer, J. Solid State Chem. 26 (1978) 389.
[12] J. Gibner, I. Vasilyeva, J. Therm. Anal. 53 (1998) 151.
[13] I. Vasilyeva, R. Nikolaev, J. Alloys Compd. 452 (2008) 94.
[14] G. Snyder, M. Christensen, E. Nishibori, T. Caillat, B. Iversen, Nat. Mater. 3 (2004) 458.
[15] G. Moh, Top. Curr. Chem. 76 (1978) 108.
[16] V.V. Malakhov, I.G. Vasilyeva, Russ. Chem. Rev. 77 (2008) 351.
[17] S. Gordienko, B. Phenochka, G. Viksman, Thermodynamics of Lantanoid Compounds, Naukova Dumka, Kiev, 1979 33 pp..